Engineered Science
DOI: https://dx.doi.org/10.30919/es1386

Molecular Dynamics and Docking Simulations in Exploring a Potential Extracellular Matrix-Based Antibiofilm: Fighting the Resistant Pseudomonas aeruginosa-Candida albicans

Rilia Faradini Putri,[1] Muhammad Ikhlas Abdjan,[2] Dewi Santosaningsih,[3] Yatim Lailun Ni'mah,[4] Nikita Putri,[5] Fatiha Khairunnisa,[1] Muji Harsini[1] and Afaf Baktir[1, 6,*]

Abstract

Glycosyltransferase activity of Bgl2 which mediates 1,3 beta-glucan biosynthesis, and phosphomannomutase/phosphoglucomutase (PMM/PGM) which catalyzes the synthesis of precursors for alginate and the O-antigen chain of lipopolysaccharide, are key enzymes in *C. albicans* and *P. aeruginosa*, respectively. These enzymes facilitate the synthesis of extracellular matrix components in biofilms. This study aimed to identify potential ligands *in silico* that demonstrate conformational fitness with the active sites of both Bgl2 and PMM/PGM, and to experimentally determine their inhibitory effects on the extracellular matrix formation in *C. albicans-P. aeruginosa* mix biofilms. Additionally, the study evaluated the effects of these ligands in combinatorial antibiofilm treatments with fluconazole and meropenem. Molecular docking and molecular dynamics (MD) simulations predicted glucosamine to act as a competitive inhibitor of both Bgl2 and PMM/PGM. The dynamic behavior of glucosamine indicated stable binding within the active site pockets of these target proteins. *In vitro* experiments demonstrated that glucosamine inhibited the formation of the extracellular matrix in *C. albicans*, *P. aeruginosa*, and *C. albicans-P. aeruginosa* biofilms by 76.5%, 51.0%, and 45.1%, respectively. Furthermore, glucosamine enhanced the efficacy of fluconazole and meropenem against *C. albicans-P. aeruginosa* biofilms. The combination of fluconazole (8-fold MIC) and meropenem (1-fold MIC) resulted in the highest and complete suppression.

Keywords: Candida albicans; Pseudomonas aeruginosa; Polymicrobial biofilms; Resistance; Antibiofilm; Glucosamine; Computational study.
Received: 02 November 2024; Revised: 18 December 2024; Accepted: 07 January 2025.
Article type: Research article.

1. Introduction

Co-infection by two major pathogens, *Candida albicans* and *Pseudomonas aeruginosa*, is frequently observed in ventilator-associated pneumonia, otitis media, cystic fibrosis, and other infectious diseases, where the pathogens can form a polymicrobial biofilm. The associated virulence factors are the glycosyltransferase activity of Bgl2 mediating 1,3 beta-glucan biosynthesis and the phosphomannomutase/phosphoglucomutase (PMM/PGM), which catalyzes the synthesis of precursors required for the biosynthesis of alginate and the O-antigen chain of lipopolysaccharide.[1] These two enzyme activities are key to the problem and are the primary targets of this study.

C. albicans and *P. aeruginosa* tend to be co-isolated from clinical samples and have been shown to interact in multiple modes within polymicrobial biofilms (PMBFs). Co-infection by *C. albicans* and *P. aeruginosa* has been identified as the leading cause of high mortality among nosocomial infections. Among the infectious diseases caused by bacterial and fungal PMBFs, *P. aeruginosa* plays a significant role alongside *C. albicans*. Additionally, viruses and parasites can interact with

[1] *Chemistry Study Program, Faculty of Science and Technology, Universitas Airlangga, Surabaya, 60115, Indonesia*
[2] *Department of Chemistry, Faculty of Mathematics and Natural Science, Universitas Negeri Surabaya, 60231, Indonesia*
[3] *Department of Clinical Microbiology, Faculty of Medicine, Brawijaya University, Malang, 65145, Indonesia*
[4] *Chemistry Department, Faculty of Science and Data Analytics, Institut Teknologi Sepuluh Nopember, Surabaya, 60111, Indonesia*
[5] *Departement of Chemistry Education, Faculty of Teacher Training and Education, Universitas Mataram, Mataram, 83125, Indonesia*
[6] *Research Group of Biochemical Engineering, Enzyme Biotechnology & Gene Cloning, Surabaya, 60115, Indonesia*
* Email: afaf-b@fst.unair.ac.id (A. Baktir)

both bacteria and fungi within PMBFs.[2] A biofilm is a heterogeneous community of microorganisms attached to abiotic or biotic surfaces or to each other, forming cell aggregates covered by a self-produced extracellular matrix (ECM) and creating a complex 3D structure.[3] The ECM chemically and physically protects the microbes from adverse actions of host immunity and antimicrobial agents. PMBFs, consisting of mixed microbial species, are the dominant form of microbial life in nature. Crosstalk through quorum sensing between *C. albicans* and *P.* aeruginosa has been reported to induce resistance to widely used antifungals.[4]

Antimicrobial combination therapy against *C. albicans* - *P. aeruginosa* biofilms does not provide maximum efficacy, even at very high doses, up to 256-fold the minimum inhibitory concentration (MIC), after 24 hours of treatment.[5] Moreover, administering very high doses of antimicrobials beyond clinically approved levels is highly toxic to humans. To devise effective treatment approaches, compounds that inhibit ECM formation in *C. albicans* and *P. aeruginosa* biofilms, when combined with antibiotic therapy, are hypothesized to demonstrate synergistic effects. A previous *in silico* screening study by our group predicted certain compounds, including glucosamine, which could compete with the substrate for the active site of the Bgl2 enzyme through docking analysis using AutoDock Vina and AutoDock4.[6] *In vitro* experiments later confirmed the inhibitory activity of glucosamine against Bgl2, suppressing ECM formation in C. albicans biofilms and enhancing the effectiveness of antifungal treatment.[7] However, ligands that inhibit ECM components of *P. aeruginosa* biofilms have not yet been reported.

In this study, a bottom-up approach was developed to identify a potent ECM-based antibiofilm agent by analyzing, *in silico*, the docking of glucosamine to the phosphomannomutase (PMM) / phosphoglucomutase (PGM) of AlgC enzyme, which is a bifunctional enzyme required to synthesize precursors for the biosynthesis of alginate exopolysaccharides and lipopolysaccharides (LPS) in *P. aeruginosa* biofilms. The results of this docking study were compared with those of L-tartaric acid (TLA), a ligand and the original substrate of PMM/PGM. Prediction of the competitive inhibitory activity of glucosamine against PMM/PGM, as determined through docking studies, was further supported by *in vitro* assays demonstrating its inhibitory activity on ECM formation.

The global increase in antibiotic resistance and the high mortality rates associated with ventilator-associated pneumonia (VAP) have prompted a search for novel therapeutic strategies to combat pneumonia, particularly VAP polymicrobial infections. Addressing this issue, a novel strategy is reported here, using glucosamine as an antibiofilm agent targeting the PMBFs of *C. albicans* and *P. aeruginosa*. Additionally, its synergistic effects in inhibiting PMBF formation were demonstrated through the administration of a combination of antimicrobials, fluconazole, and meropenem as an effort to overcome resistance to antimicrobial therapy.

2. Experimental section

2.1 Structural preparation

The structure of BgL2 (PDB ID: 1EQC) and PMM/PGM (PDB ID: 1K2Y), selected as the target biomolecules, were obtained from the Protein Data Bank. These biomolecules are produced by *C. albicans*.[8] and *P. aeruginosa*,[9] respectively. The protonation states of all ionizable amino acid residues were calculated at pH 7.0 using the H++ web server (http://newbiophysics.cs.vt.edu/H++/). Moreover, castanospermine (CTS) and L(+)-tartaric acid (TLA) bind to the pocket site of each target, respectively. Specifically, the 1K2Y structure contains a zinc ion (Zn^{2+}) that binds to its pocket site. Native ligand coordinates were extracted using Chimera 1.13 software to determine the pocket site of the target protein. Glucosamine (Glu) was chosen as a potential inhibitor due to its availability and safety for antimicrobial therapy. The electrostatic potential (ESP) charge of Glu was calculated using the semi-empirical quantum Austin model-1 (SQM-AM1) method. Additionally, the Antechamber and AMBER FF14SB force field was used to calculate several parameters, such as restrained charge, bonded, and non-bonded interactions.

2.2 Pharmacokinetic properties

The modeled compounds (CTS, TLA, and Glu) in this study were used to predict their pharmacokinetic properties, including drug-likeness, bioavailability, and ADMET (absorption, distribution, metabolism, excretion, and toxicity). The input files in SMILES format were used for these predictions. The SwissADME web service was employed to calculate the bioavailability and drug-likeness of the modeled compounds.[1] Meanwhile, the pkCSM server was used to predict their ADMET properties.[2]

2.3 Molecular docking

Molecular docking was performed using the Dock6 package through redocking and docking analysis. The redocking step aimed to determine the pocket site based on the native ligand coordinates. Several crucial parameters, such as grid spacing, center, and dimensions, were applied for successful redocking. Specifically:

- 1EQC: grid spacing = 0.3 Å, center (X: 36.44, Y: 39.12, Z: 58.01), dimensions (X: 13.67, Y:11.14, Z: 16.69).
- 1K2Y: grid spacing = 0.1 Å, center (X: 53.57, Y: 48.72, Z: 13.24), dimensions (X: 22.79, Y: 23.87, Z: 18.07).

The energy interaction was described using gas terms, followed by grid score (GS), van der Waals (EvdW), and electrostatic (Eele) energies.[10,11] The redocking step was considered acceptable if the RMSD value was below 2.0 Å.[11] The parameters obtained from redocking were used to determine the initial conformation of Glu against the target protein.

2.4 Molecular dynamics simulation

The initial conformation from molecular docking was further evaluated using molecular dynamics (MD) simulation.[12] The MD simulation steps were performed with the Amber18 and AmberTools19 packages. The tleap tool was used for topology preparation for each system.[13] Key parameters in topology preparation included TIP3PBOX solvate box (distance: 10 Å) and sodium ions (Na^+). The 1K2Y system contained a Zn^{2+} ion in the pocket site. To generate parameters and coordinates for Zn^{2+}, the 12-6-4 Lennard-Jones (LJ) non-bonded AMBER force field (frcmod.ions234lm_1264_tip3p) was applied. The solvated topology was minimized through three steps:

1. Water and ion minimization,
2. Ligand-receptor minimization,
3. Whole system minimization.

The steepest descent (maxcyc: 4500 steps) and conjugate gradient (ncyc: 1500 steps) methods were applied. Subsequent steps included heating, equilibration, and production.[14]

- The heating step ran for 200 ps, gradually increasing from 0 K to 310 K.
- The system was equilibrated in four steps with restraint forces of 30, 20, 10, and 5 kcal/mol for a total of 1300 ps.
- After equilibration, each system was simulated under periodic boundary conditions with the NPT ensemble (310 K, 1 atm) for up to 100 ns. The MD trajectory was saved every 1000 ps during production for analysis.

The generated trajectories were analyzed for:

- Root-mean-square deviation (RMSD)
- Radius of gyration (RoG)
- Complex conformation
- Root-mean-square fluctuation (RMSF)
- Hydrogen bonds (H-bonds)
- Solvent-accessible surface area (SASA)
- Radial distribution function (RDF)
- Free energy binding (ΔG_{bind})
- Energy decomposition ($\Delta G_{bind}^{residue}$)

Free energy binding (ΔG_{bind}) and energy decomposition ($\Delta G_{bind}^{residue}$) were calculated using 2000 MD snapshots from the last 20 ns of trajectories. The molecular mechanics-generalized born surface area (MM-GBSA) method was applied.[15] The estimation of ΔG_{bind} included enthalpy (ΔH) and entropy change ($-T\Delta S$) (Eq. (1)). The $-T\Delta S$ term was ignored due to computational cost. Changes in conformational entropy were ignored when only relative binding free energies of similar ligands were needed. The ΔH term consisted of gas-phase free energy (ΔG_{gas}) and solvation energy (ΔG_{solv}) (Eq. (2)). The ΔG_{gas} was influenced by Eq. (3):

- Van der Waals energy (ΔE_{vdW})
- Electrostatic energy (ΔE_{ele})
- Bonded energy (ΔE_{bonded})

The ΔE_{bonded} included bond, angle, and torsion energies, which were negligible. The ΔG_{solv} included:

- Generalized Born electrostatic solvation energy (ΔG_{solv}^{ele})
- Nonpolar solvation energy ($\Delta G_{solv}^{nonpolar}$) (Eq. (4))

Finally, all energy components contributed to ΔG_{bind} (Eq. (5)).

$$\Delta G_{bind}=\Delta H-T\Delta S \quad (1)$$

$$\Delta G_{bind}=\Delta G_{gas}+\Delta G_{Solv}-T\Delta S \quad (2)$$

$$\Delta G_{gas}=\Delta E_{vdw}+\Delta E_{ele}++\Delta E_{bonded} \quad (3)$$

$$\Delta G_{Sol}=\Delta G_{solv}^{ele}+\Delta G_{Solv}^{Nonpolar} \quad (4)$$

$$\Delta G_{bind}==\Delta E_{vdw}+\Delta E_{ele}+\Delta G_{solv}^{ele}+\Delta G_{Solv}^{Nonpolar} \quad (5)$$

2.5 Microbial strains and culture conditions

P. aeruginosa ATCC 27853 and *C. albicans* ATCC 14053 were rejuvenated on solid Sabouraud dextrose agar (SDA) and tryptic soy agar (TSA) media, respectively. A single colony from each rejuvenated solid culture was suspended in PBS to obtain 100 µL of each microbial suspension. The suspensions were inoculated in 20 mL of yeast peptone dextrose (YPD) or tryptic soy broth (TSB) and then incubated on a rotary shaker at 150 rpm and 37 °C to obtain the *C. albicans* and *P. aeruginosa* inocula respectively. For the planktonic and biofilm assays, the Roswell Park Memorial Institute-1640 (RPMI-1640) medium (Sigma-Aldrich, USA) was used.

2.6 Biofilm preparation

Planktonic cultures (inocula) of *C. albicans* and *P. aeruginosa* were centrifuged at 3,000 g, 4 °C for 10 minutes, and the cell pellets were resuspended in RPMI-1640 until suspensions of 10^7 cells/mL were obtained. A cover glass was inserted into the well of a 24-well microtiter plate, the microbial suspensions with or without glucosamine and antimicrobials were added, and then the plate was incubated at 37 °C for 48 hours.

2.7 Measurement of MIC of fluconazole and meropenem against planktonic cells

The MIC of single and combined antimicrobial agents was determined using the liquid microdilution method according to the European Committee on Antimicrobial Susceptibility Testing (EUCAST). The MIC of a single antimicrobial agent was determined against a single microbial planktonic cell, while the combined antimicrobial agents were tested against polymicrobial planktonic cells. The susceptibility of each planktonic cell culture to antimicrobials was determined based on the MIC value.

The single microbial suspension was at 10^6 cells/mL, while the polymicrobial suspension was 2×10^6 cells/mL. The suspensions were each added to the wells of 96-well microtiter plates with the antimicrobial solution in a ratio of 1:2 so that the final suspension was 5×10^5 cells/mL. Then, the antimicrobial solution in RPMI-1640 was added to each well in a twofold series.

The negative controls in this experiment included RPMI-1640 medium, antimicrobial solution, and PBS as the antimicrobial solvent. The microtiter plate was then incubated at 37 °C overnight. The MIC was determined by visually observing the turbidity gradient, which indicated the capacity of the planktonic cell population to grow in the presence of antimicrobials. The minimum concentration at which growth inhibition occurred was equivalent to the MIC.[5]

2.8 Assessment of glucosamine effects

The effect of glucosamine on the efficacy of the fluconazole-meropenem combination in eradicating *C. albicans-P. aeruginosa* PMBFs were assessed by measuring the colony-forming units (CFUs), performing the crystal violet assay, and using scanning electron microscopy (SEM).

2.9 Measurement of the biofilm ECM by crystal violet assay

Aliquots of the suspensions of the single and PMBFs at 10^7 cells/mL (100 µL each) were pipetted into different wells of a 96-well microtiter plate. The suspension for the PMBF consisted of 50% *C. albicans* and 50% *P. aeruginosa*, while the single biofilm consisted of 100% of each cell type. The microtiter plate was then incubated at 37 °C for 90 minutes to allow the cells to adhere to each well, and then carefully washed twice with PBS.

Control experiments were also carried out to grow single and PMBFs, with ligand solution and RPMI-1640. Then, 100 µL of 0.1 g/mL glucosamine was added to each well to evaluate its potential as an antibiofilm agent. Meanwhile, 100 µL of RPMI-1640 was added only to the growth control well, and the microtiter plate was incubated again for 48 hours. The biofilm formed in each well was washed twice with PBS and then fixed with 100 µL of methanol for 15 minutes. Next, the 96-well microtiter plate was dried, and 125 µL of 0.1% crystal violet was added to each well, incubated for 5 minutes, and then washed with 100 µL of PBS. Finally, 100 µL of 30% acetic acid was added, incubated for 10 minutes, and the OD595 was read.

2.10 Determination of CFUs

The suspensions of 50% *C. albicans* and 50% *P. aeruginosa* were mixed. Then, 100 µL of the mixture was pipetted into a 96-well microtiter plate and incubated at 37 °C for 90 minutes. For biofilm formation, 100 µL of RPMI-1640 was added to each well and incubated for 24 hours. The planktonic suspension was discarded, and the lost volume was replaced with a solution containing RPMI-1640, glucosamine, and an antimicrobial agent with increasing concentrations (up to 8-fold of the MIC). The 96-well microtiter plate was then incubated at 37 °C for 60 hours. Every 12 hours, a specific volume was sampled from each well for CFU, SEM, and MIC analysis. The lost volume was replaced with a fresh mixture of ligand and antimicrobial solution.

The determination of CFUs of the microorganisms was conducted using the spread-plate method on suitable selective solid media. SDA supplemented with 0.1% of the antimicrobial meropenem was used to cultivate *P. aeruginosa*, while TSA supplemented with 0.1% of the antifungal fluconazole was used to cultivate *C. albicans*. The total plate count was then used to calculate the CFUs.

2.11 Observation of biofilm morphology using SEM

A coverslip was inserted into the well of a 24-well microtiter plate. Microbial suspensions with or without glucosamine and antimicrobials were added and incubated at 37 °C for 48 hours. The biofilm formed on the surface of the coverslip was carefully washed twice with sterile PBS and fixed with 2.5% (w/v) glutaraldehyde in cacodylate buffer overnight or for 24 hours. The biofilm was dehydrated using methanol for 30 minutes and then coated with Au/Pd. The sample was thus ready for observation using SEM.

3. Results and discussion

Synthesis and metabolic enzymes that contribute to the formation of the ECM in the *C. albicans-P. aeruginosa* PMBF are BgL2 and PMM/PGM. BgL2 catalyzes the conversion of glucose to β-1,3-glucan, a key component of the *C. albicans* biofilm ECM. PMM/PGM belongs to the subclass of phosphohexomutases and catalyzes the formation of mannose-1-phosphate from glucose-6-phosphate or mannose-6-phosphate. Mannose-1-phosphate is a precursor in the synthesis of exopolysaccharide alginate, a constituent of the biofilm matrix and the O-antigen of LPS, both of which are associated with *P. aeruginosa* virulence. Other constituents of the ECM include rhamnolipids and various exopolysaccharides.

An antibiofilm strategy that prevents ECM formation has emerged as one of the most promising approaches in recent years to eradicate tolerant microorganisms in biofilms, which are otherwise difficult to manage.[16] Therefore, a novel ECM-based antibiofilm compound was designed to act as a competitive inhibitor of virulence-contributing enzymes in microbial pathogens. This strategy can also target other biomolecules, such as receptors that play essential roles in microbial virulence.

In this context, glucosamine (GlcN) was evaluated *in silico* as a potential inhibitor by assessing its ability to bind to target biomolecules based on binding energy values. The structural similarity of GlcN to known biofilm inhibitors, such as Castanospermine and L(+)-Tartaric acid, provides a distinct advantage. This similarity may enhance the likelihood of GlcN adopting the binding conformation of known inhibitors at the protein's binding pocket. A smaller (more negative) binding energy value indicates an enhanced ability to form a stable complex with the target biomolecule. Furthermore, glucosamine was tested *in vitro* and *in vivo* for its potential as an antibiofilm agent (Fig. 1).

3.1 Drug-likeness, bioavailability and pharmacokinetic predictions

The modeled compounds' pharmaceuticals can be evaluated based on their moiety through bioavailability and drug-likeness. The results indicate that Glu is a promising therapeutic candidate that fulfill several drug-likeness criteria and show similar properties toward CTS and TLA as references/standards (Table S1). The oral bioavailability analysis provides clear insights into the physicochemical properties of the modeled compound (Fig. 2). According to the oral bioavailability is generally expected to meet the following criteria: flexibility (0 < number of rotatable bonds < 9), polarity (20 Å² < TPSA < 130 Å²), lipophilicity (−0.7 < X log P3 < 5.0), size (150 D < MW < 500 D), insaturation (0.25 < Csp^3 < 1), and solubility (-6 < log S < 0).[2] Moreover, the Lipinski rules perform no violations for the Glu as a drug candidate. The findings indicate that the Glu meets all the requirements of drug-likeness and oral bioavailability. This suggests that Glu has greater potential for use as oral medication similar to the reference compounds.

ADMET prediction helps provide drug information when entered into the body. This information is useful for redicting the pharmacokinetic properties of potential drugs. Several crucial ADMET parameters are Caco-2 permeability, h uman small intestine (HIA), blood-brain barrier (BBB), total clearance, cytochrome isoenzymes (CYP), *Salmonella typhimurium* reverse mutation assay (AMES) toxicity, and hepatotoxicity, and skin sensitization.[1,3] In detail, the information on ADMET properties of modeled compounds is provided in Table 1. Overall, the predictions of ADMET for the Glu show promising potential as a drug candidate. The results show that the Glu is well-absorbed in human intestines (+HIA: 35.37%). Moreover, the Glu does not cross the BBB to assess its permeability. This finding indicates that Glu does not affect the nervous system.[4] In particular, for metabolism and toxicity parameters, showing the Glu does not interfere with cytochrome isoenzymes and it is identified as a non-toxic category. The Glu demonstrates strong potential as a drug candidate due to its non-interference with these enzymes and the absence of undesirable side effects during metabolic processes. The information presented in this section is initial predictions to see the pharmacokinetic properties of the Glu. However, the information presented can provide insight and initial consideration before conducting clinical trials on the ability of this compound.

3.2 Molecular docking analysis

To determine the initial coordinates of the pocket site, the redocking step provides an efficient protocol.[10] As mentioned, CTS and TLA are native ligands that serve as references for determining the initial coordinates of the target protein. The selected cluster spheres are designed to generate specific coordinates for the pocket site. During the redocking step, the docking conformation (pose) closely aligns with the co-crystal ligand coordinates. This alignment is demonstrated by the superposition with an RMSD value below 2.0 Å for each native ligand (Fig. S1). This result confirms that the conformation of the native ligand within the pocket site is accurate. Confidently, these coordinates and parameters can be used to dock the Glu molecule to 1EQC and 1K2Y as target proteins. Notably, the lowest dock score or grid score indicates

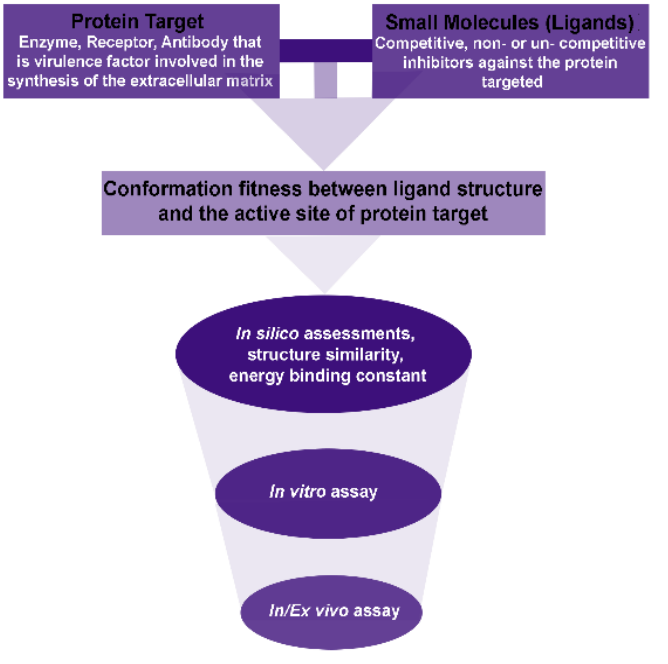

Fig. 1: Computational design of ECM-based antibiofilm.

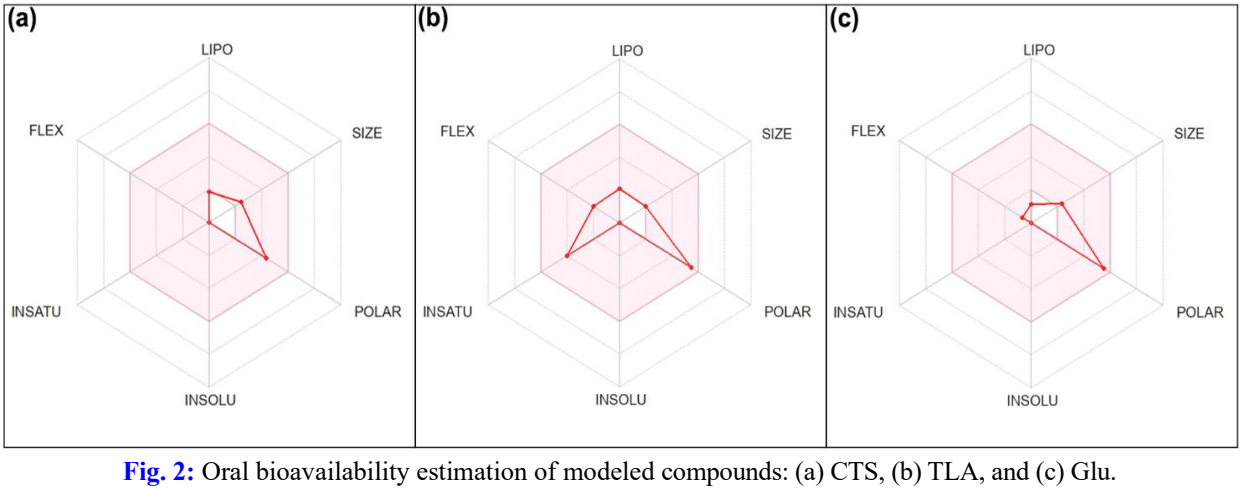

Fig. 2: Oral bioavailability estimation of modeled compounds: (a) CTS, (b) TLA, and (c) Glu.

Table 1: Results of ADMET predictions using pkCSM webserver.

Parameters	CTS	TLA	Glu
Absorption:			
[a]Caco-2	0.36	-0.50	-0.43
[b]HIA	58.01	4.27	35.57
Distribution:			
[c]BBB	-0.96	-1.10	-1.11
Metabolism:			
CYP1A2 Inhibitor	No	No	No
CYP2C19 Inhibitor	No	No	No
CYP2C9 Inhibitor	No	No	No
CYP2D6 Inhibitor	No	No	No
CYP3A4 Inhibitor	No	No	No
Excretion:			
[d]Total Clearance	0.86	0.87	0.72
Toxicity:			
AMES Toxicity	No	No	No
Hepatotoxicity	No	No	No
Skin Sensitization	No	No	No

[a]Hight Caco-2 permeability > 0.90 (log Papp in 10^{-6} cm/s), [b]Intestinal Absorption-Human (+HIA > 30% and -HIA < 30%), [c]BBB Permeability (+log BB > 0.30 and -log BB < -1.00), and [d]Total clearance (log mL/min/Kg).

better ligand-protein binding affinity.[5] Following the analysis, we docked Glu into the target protein. The results show that Glu occupies the pocket site of each protein effectively (Fig. S2). As mentioned, the energy contribution (EvdW + Eele) in the docking interaction is calculated using a grid-based scoring function in the gas phase. The grid score (GS) provides an initial conformation for ligand-protein interactions from a thermodynamic perspective. The 1EQC-Glu complex (GS: -34.18 kcal/mol) shows stronger energy interactions compared to the 1K2Y-Glu complex (GS: -24.25 kcal/mol). This indicates that EvdW and Eele significantly contribute to the binding of all complexes (Table S2). Furthermore, the interactions between Glu and amino acid residues in the pocket site of the target proteins are shown in Fig. 3. Our investigations reveal that several amino acid residues interact with Glu through hydrogen bonds, carbon-hydrogen bonds, and unfavorable donor-donor interactions. Hydrogen bonds (H-bonds) play a crucial role in maintaining the stability of ligand binding to the target proteins.[17,18] Specifically, the amino acid residues involved in these interactions include:

- 1EQC-CTS: E21, Y23, N185, E186, E286, and W357
- 1EQC-Glu: E21, Y23, N140, E186, E286, and L298
- 1K2Y-TLA: H109, K118, and R247
- 1K2Y-Glu: D18 and H308

These results indicate that the Glu structure has advantageous properties due to its similarity to the native ligands of each protein (Table S2). This similarity lies in the molecular size and functional groups (-OH and -NH_2).

Based on our investigation, we conclude that Glu shows promising potential as an inhibitor of BgL2 and PMM/PGM proteins. However, molecular docking provides only preliminary data on the coordinates of Glu binding to the pocket site. The data generated from molecular docking can sometimes reflect relatively rigid structures concerning interaction energy calculations in the gas phase.[10,11]

Therefore, further analysis of binding affinity and ligand-protein interactions should be conducted through molecular dynamics (MD) simulation. Integrating molecular docking with MD simulation is an efficient protocol for studying protein-ligand behavior under conditions that approximate physiological environments.[12,19] Hopefully, this study and exploration of Glu as a potential inhibitor of these two proteins will yield the expected conclusions during *in vitro* testing.

3.3 Dynamics conformation: stability, rigidity, flexibility, and mobility

The trajectory production stage was performed for 100 ns on each system. For evaluation purposes, both the apo-protein (1EQC and 1K2Y) and complex (1EQC-Glu and 1K2Y-Glu) systems were simulated. The goal was to observe the dynamic behavior of the proteins with and without the Glu molecule. Trajectories generated over 100 ns were analyzed using the cpptraj tool available in the AmberTools19 package.[20] The analyzed variables included RMSD, RoG, RMSF, and inhibitor mobility.

System stability was assessed based on RMSD fluctuations during the simulation.[21] We performed RMSD analysis and examined its distribution for each frame (Fig. 4) to determine the stability levels of the apo-protein and the complexes. A total of 10,000 frames were analyzed over 100 ns. The data show that all systems exhibited good stability (RMSD ≤ 0.35 nm). Additionally, the RMSD distribution indicates that the 1EQC and 1EQC-Glu systems have better stability compared

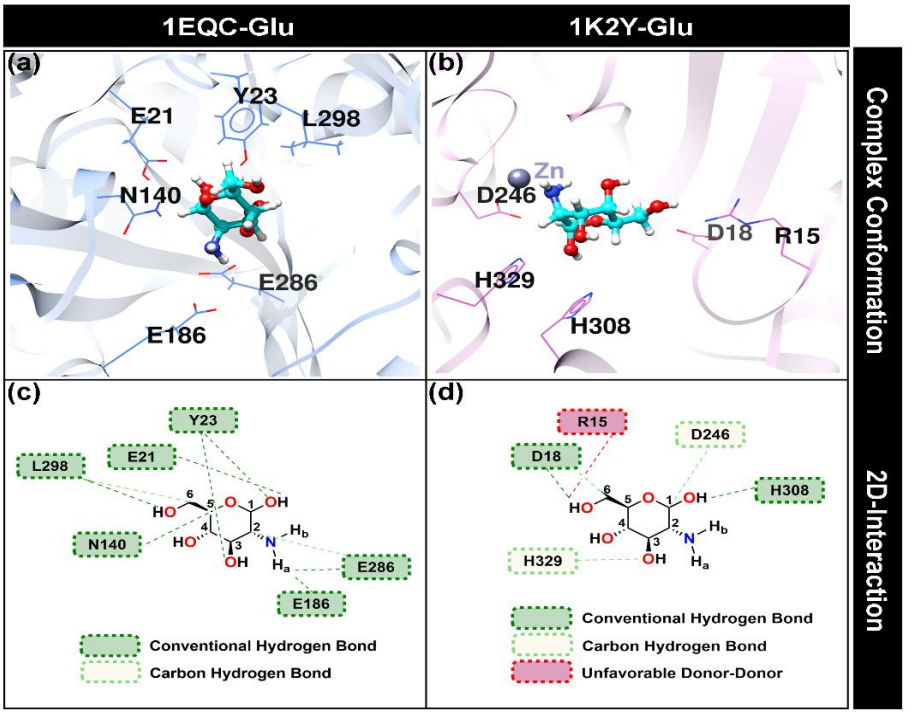

Fig. 3: The protein-glucosamine interaction represented by complex conformation for (a) 1EQC-Glu, (b) 1K2Y-Glu and 2D interaction, (c) 1EQC-Glu, and (d) 1K2Y-Glu.

to the 1K2Y and 1K2Y-Glu systems. Specifically, the RMSD distribution values for each system are:

- 1EQC: 0.14–0.19 nm
- 1EQC-Glu: 0.14–0.21 nm
- 1K2Y: 0.18–0.32 nm
- 1K2Y-Glu: 0.16–0.34 nm

We found that the 1K2Y-Glu system showed higher RMSD fluctuations compared to the other systems. Therefore, further investigation is needed to ensure that the Glu molecule remains within the 1K2Y pocket site. Nevertheless, all systems achieved good stability, as indicated by the relatively low RMSD fluctuations.

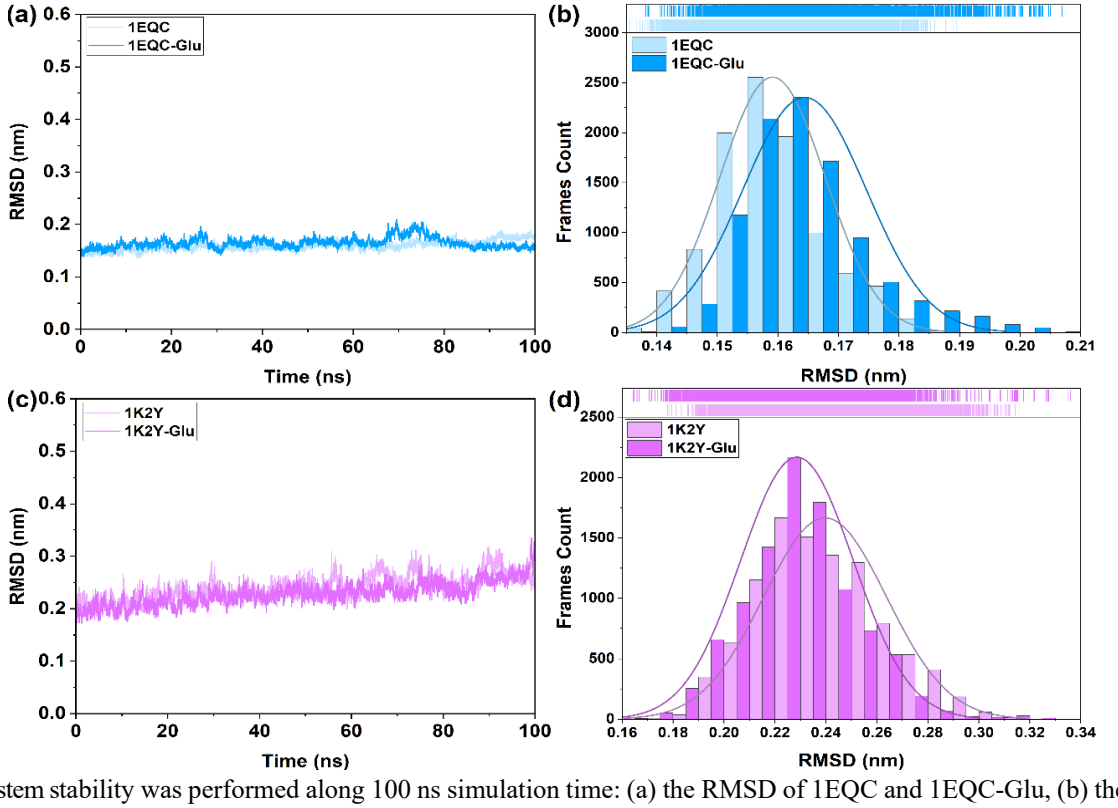

Fig. 4: The system stability was performed along 100 ns simulation time: (a) the RMSD of 1EQC and 1EQC-Glu, (b) the distribution of 1EQC and 1EQC-Glu, (c) the RMSD of 1K2Y and 1K2Y-Glu, and (d) the distribution of 1K2Y and 1K2Y-Glu.

Following the analysis, the radius of gyration (RoG) was investigated to assess the system's rigidity based on its structure. The RoG value reflects the compactness of the structure.[22] Consistent with system stability (Fig. 4), the 1EQC and 1EQC-Glu systems exhibit better compactness compared to the 1K2Y and 1K2Y-Glu systems. This is supported by the average RoG values for each system:

- 1EQC: 2.02 ± 0.00 nm
- 1EQC-Glu: 2.02 ± 0.00 nm
- 1K2Y: 2.28 ± 0.01 nm
- 1K2Y-Glu: 2.27 ± 0.02 nm (Fig. S3)

Overall, all systems maintained good structural compactness throughout the 100 ns simulation. This compactness is visualized by the average structure extracted from the trajectories (Fig. 5). Additionally, we investigated the flexibility of amino acid residues within the pocket site of each targeted protein to observe the influence of Glu binding. The RMSF value was used to identify the flexibility of residues within a 5 Å radius of the Glu coordinates. Our findings indicate that the presence of Glu in the pocket site stabilizes the protein-glucosamine interaction, as shown by the lower RMSF values in the complex systems compared to the apo-protein systems (Fig. 4). Therefore, we conclude that the binding of the Glu molecule in the pocket site of the targeted proteins enhances system stability.

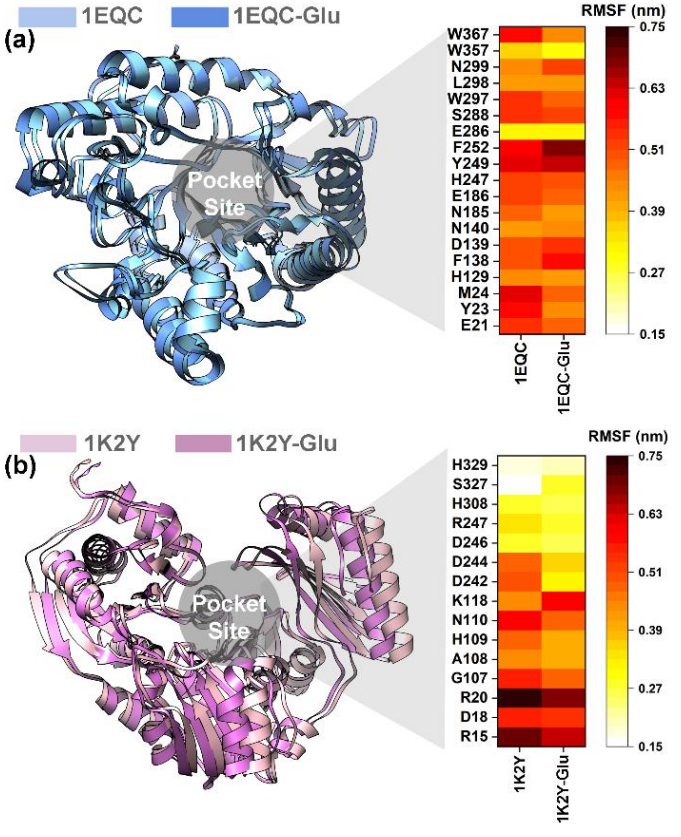

Fig: 5: The average structure of each system was superposed to perform its compactness. The RMSF was performed to calculate the flexibility of the targeted protein pocket site. (a) 1EQC and 1EQC-Glu and (b) 1K2Y and 1K2Y-Glu.

In addition to investigating the inhibitor mobility at the pocket site, we visualized the Glu mobility every 20 ns during the 100 ns simulation (Fig. 6). This analysis was performed to confirm that the Glu molecule remains bound to the pocket site. The visualization illustrates how the conformation of the target protein structure changes throughout the simulation. Consistent with the previous analysis (stability and rigidity), the results show that the protein structure did not undergo significant changes. Furthermore, Glu remained within the pocket site throughout the simulation. This is evident from the Glu mobility at the 1EQC pocket site, where it did not experience significant movement and remained well-occupied at the pocket site. In contrast, Glu showed some mobility at the 1K2Y pocket site; however, it remained within the pocket site and did not leave it. Additionally, the amino acid residue colored yellow indicates that no significant conformational changes occurred. These findings provide insight into how Glu can maintain its position and effectively bind to the pocket sites of the BgL2 and PMM/PGM proteins.

3.4 Molecular interaction on the pocket site: hydrogen bond and water accessibility

To understand the reason why Glu can bind very well to the pocket site of the targeted protein, the hydrogen bond and water accessibility were investigated. The analysis was performed using 10,000 frames extracted from 100 ns of trajectories. These variables aim to examine the molecular interactions at the pocket site of each system.

Hydrogen bonds (H-bonds) play a crucial role in ligand-protein interactions by maintaining complex stability.[17,23] The presence of –OH and –NH2 groups in the Glu molecule enhances its ability to increase H-bond interactions as hydrogen donors or acceptors. Note that the H-bond analysis is calculated by considering the number of frames recorded during the simulation time. It is recorded as the presentation of hydrogen bonds (PHB), which represents the number of frames recorded divided by the total number of frames. The highest PHB value indicates the likelihood of an intense H-bond interaction being formed. Additionally, the H-bonds considered in this analysis are those with a PHB percentage above 10% (Table 2). The results show that Glu forms a more intense H-bond interaction with the 1EQC protein than with 1K2Y. This can be seen from the number of H-bonds recorded during the simulation time (Fig. S4) and reinforced by the PHB value. This finding also correlates with the molecular docking results, which show similar findings (Table S1).

It should be noted that during the simulation, each atom in the system moves dynamically,[24] which leads to the detection and undetection of several H-bond interactions. For example, in the molecular docking analysis of 1K2Y-Glu, Glu interacts with residue H308. However, in the MD simulation, this interaction was not detected. This is understandable because Glu's mobility (Fig. 5) was quite intense in the 1K2Y pocket site during the simulation. As a result, the possibility of an H-bond forming with residue H308 is smaller. Overall, the

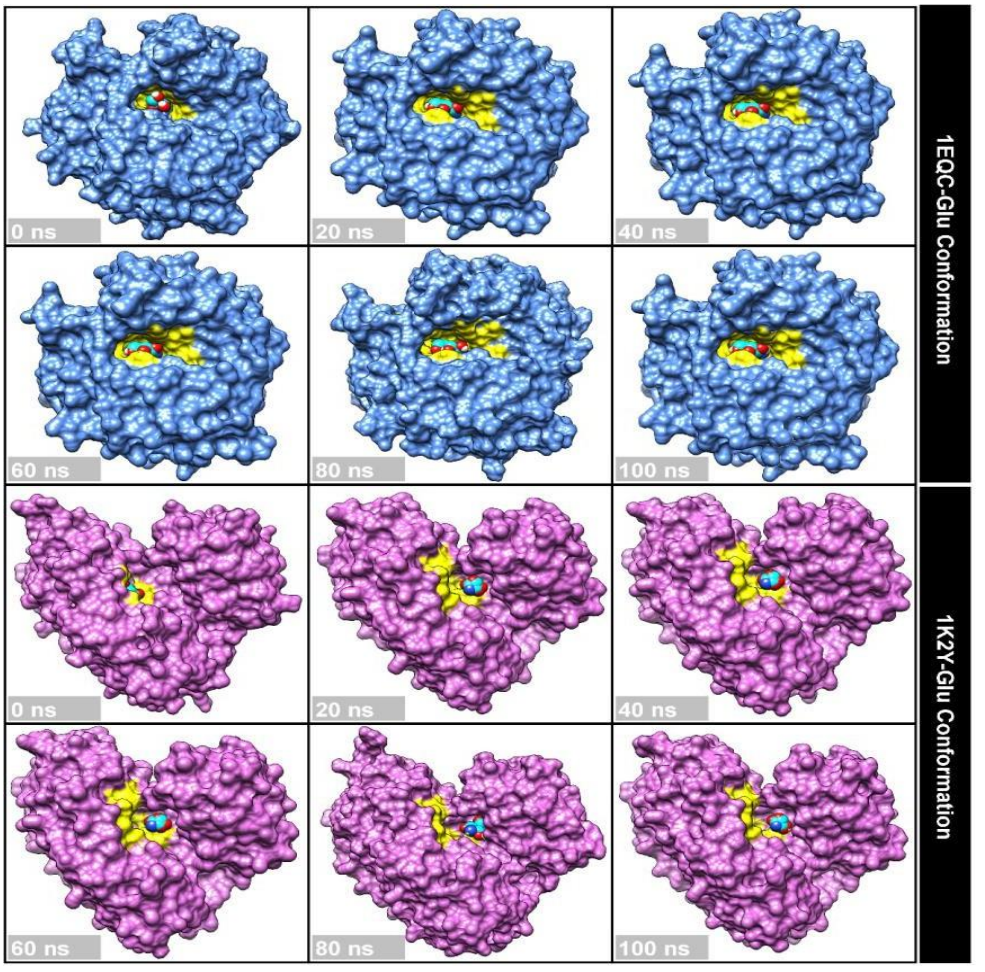

Fig. 6: Glucosamine mobility on the targeted protein surfaces during the simulation. Initial coordinated (radius: 5 Å) was identified by yellow color.

Table 2: Hydrogen bond analysis using 10,000 frames from 100 ns of trajectories of IEQC-Glu (A) and 1K2Y-Glu (B) Complexes (Cutoff values: distance (3.5 Å) and angle (120°)).

Donor#H…Acceptor	Frames	Dist. (Å)	Angle (o)	PHB (%)
(A) 1EQC-Glu Complex				
(N140)HD22…OH-C6	6395	3.00	154.58	63.95
(N140)HD22…C1-O-C6	3194	3.04	137.01	31.94
(Y23)H…OH-C1	2798	2.85	161.17	27.98
(N140)H…OH-C6	2767	3.26	151.12	27.67
1C-OH…O(E286)	2727	2.66	164.06	27.27
1C-OH…O(E21)	2598	2.91	159.24	25.98
4C-OH…O(L298)	2499	2.81	160.62	24.99
3C-OH…O(E286)	2312	2.60	166.20	23.12
(Y23)H…OH-C3	2153	2.89	157.13	21.53
2C-NHa…O(E286)	2094	3.04	150.72	20.94
2C-NHb…O(E186)	1265	2.92	159.69	12.65
(B) 1K2Y-Glu Complex				
4C-OH…O(D18)	1400	2.70	160.15	14.00

H-bonds formed between Glu and the target protein lead to the same conclusion: the Glu molecule can form interactions with the amino acid residues at the pocket site in the form of H-bond interactions.

Further investigation of molecular interactions at the pocket site was conducted by examining water accessibility. This analysis aims to assess how water molecules access the pocket sites of the targeted protein. Water molecules play a crucial role in maintaining the ligand-protein structure.[25,26] The presence of water molecules at the pocket site can increase the likelihood of H-bond interactions through mediation by water molecules. Several variables were measured to address this

issue, such as the solvent-accessible surface area (SASA) and radial distribution function (RDF) (Fig. 7). The results show that 1K2Y-Glu is more easily accessible to water molecules than 1EQC-Glu, as supported by the SASA values for each system (1EQC-Glu: ~0.37 nm² and 1K2Y- Glu: ~2.63 nm²). Additionally, water molecules that approach the oxygen (O) and nitrogen (N) atoms in the Glu molecule were analyzed using RDF (g(r)), based on the integration number (n(r)) within a spherical radius (r).[27] The data on the number of water molecules is provided in Table S3. The lower hydration peaks observed in the 1EQC-Glu system, compared to 1K2Y-Glu, are shown in Fig. 7. This data aligns with the SASA values mentioned earlier, further supporting the conclusion that Glu is more accessible to water molecules in the 1K2Y pocket site. At the atomic level, the N atom shows higher hydration sensitivity. We suggest that the presence of the -NH2 group on the Glu molecule enhances its stability and maintains interactions with water molecules. This can be seen in the n(r) values for the N atom in each system: 1EQC-Glu: 2.81 and 1K2Y-Glu: 2.89. In summary, the O and N atoms in the Glu molecule enhance water accessibility. All the findings discussed in this section suggest that the Glu molecule can bind effectively to the pocket site of the targeted protein.

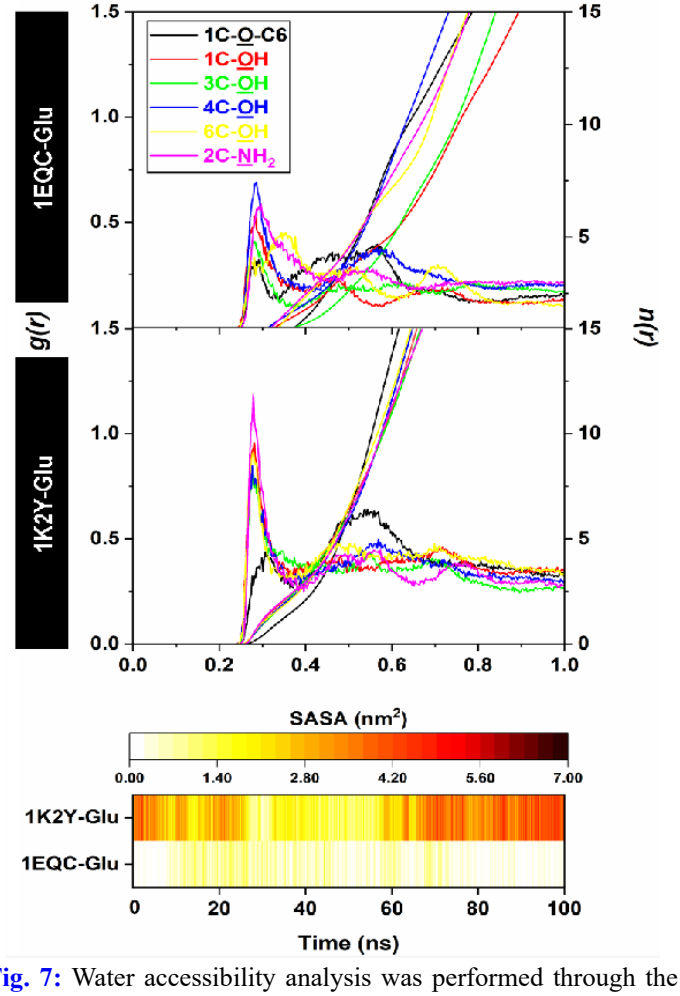

Fig. 7: Water accessibility analysis was performed through the radial distribution function (top) and the solvent-accessible surface area (bottom).

3.5 Binding affinity: Free energy binding and decomposition energy

All the findings indicate that Glu has stabilized and binds effectively to the pocket site of each targeted protein. In this section, we present the analysis for binding affinity calculations through free energy binding (ΔG_{bind}) and energy decomposition ($\Delta G_{bind}^{residue}$).[15,28] Calculations were performed using the last 20 ns of the trajectories. It was assumed that the trajectory range did not experience significant changes, which is supported by the Glu snapshot at the pocket site, where no substantial changes in coordinates were observed (Fig. S5).

Following this, the energy components of (ΔG_{bind}) are listed in Table 3. The energy values show the contribution of gas (ΔG_{gas}) and solvation (ΔG_{sol}) terms [28]. ΔG_{gas} consists of van der Waals energy (ΔE_{vdW}) and electrostatic energy (ΔE_{ele}), while ΔG_{sol} consists of the Generalized Born model/polar energy (ΔG_{solv}^{ele}) and solvent-accessible surface area/nonpolar energy ($\Delta G_{solv}^{nonpolar}$). In summary, Glu shows a stronger ΔG_{bind} with 1EQC than with 1K2Y. This is evident from the more negative ΔG_{bind} value for 1EQC-Glu compared to 1K2Y-Glu, thermodynamically. This result is primarily due to the higher contribution of ΔE_{bind} to ΔG_{bind} in each system. These findings are consistent with the GS values measured in the molecular docking section (Table S1). Overall, Glu binds very effectively to the pocket site of the targeted protein.

Table 3: Energy components (kcal/mol) of complexes calculated with MM-GBSA.

Energy components	1EQC-Glu	1K2Y-Glu
ΔE_{vdW}	-21.83 ± 0.05	-11.85 ± 0.08
ΔE_{ele}	-39.77 ± 0.14	-44.87 ± 0.27
ΔG_{gas}	-61.60 ± 0.13	-56.72 ± 0.29
ΔG_{solv}^{ele}	41.06 ±0.09	45.95 ±0.20
$\Delta G_{solv}^{nonpolar}$	-3.78 ± 0.00	-2.59 ± 0.01
ΔG_{sol}	37.28 ± 0.09	43.36 ± 0.19
ΔG_{bind}	-24.31 ± 0.08	-13.36 ± 0.12

To evaluate the contribution of amino acid residues toward binding affinity, energy decomposition ($\Delta G_{bind}^{residue}$) was calculated. This variable aims to identify the key binding residue that is responsible for stabilizing the Glu binding and it gives the details about the binding mechanism.[28] It should be noted that the amino acids considered key binding residues are those that have a $\Delta G_{bind}^{residue}$ value ≤ -0.50 kcal/mol. In detail, each system shows that several key binding residues are 1EQC-Glu (Eight residues: E21, Y23, F138, N140, Y249, F252, L298, and W357) and 1K2Y-Glu (Six residues: S327, E375, R421, S423, T426, and V430) (Fig. 8). The 1EQC-Glu interaction showed a similar correlation with molecular docking (Fig. 1). Meanwhile, 1K2Y-Glu showed quite significant changes in interaction. It has been described previously that Glu undergoes movement in the 1K2Y pocket site (Fig. 6). Therefore, MD simulation findings provide more

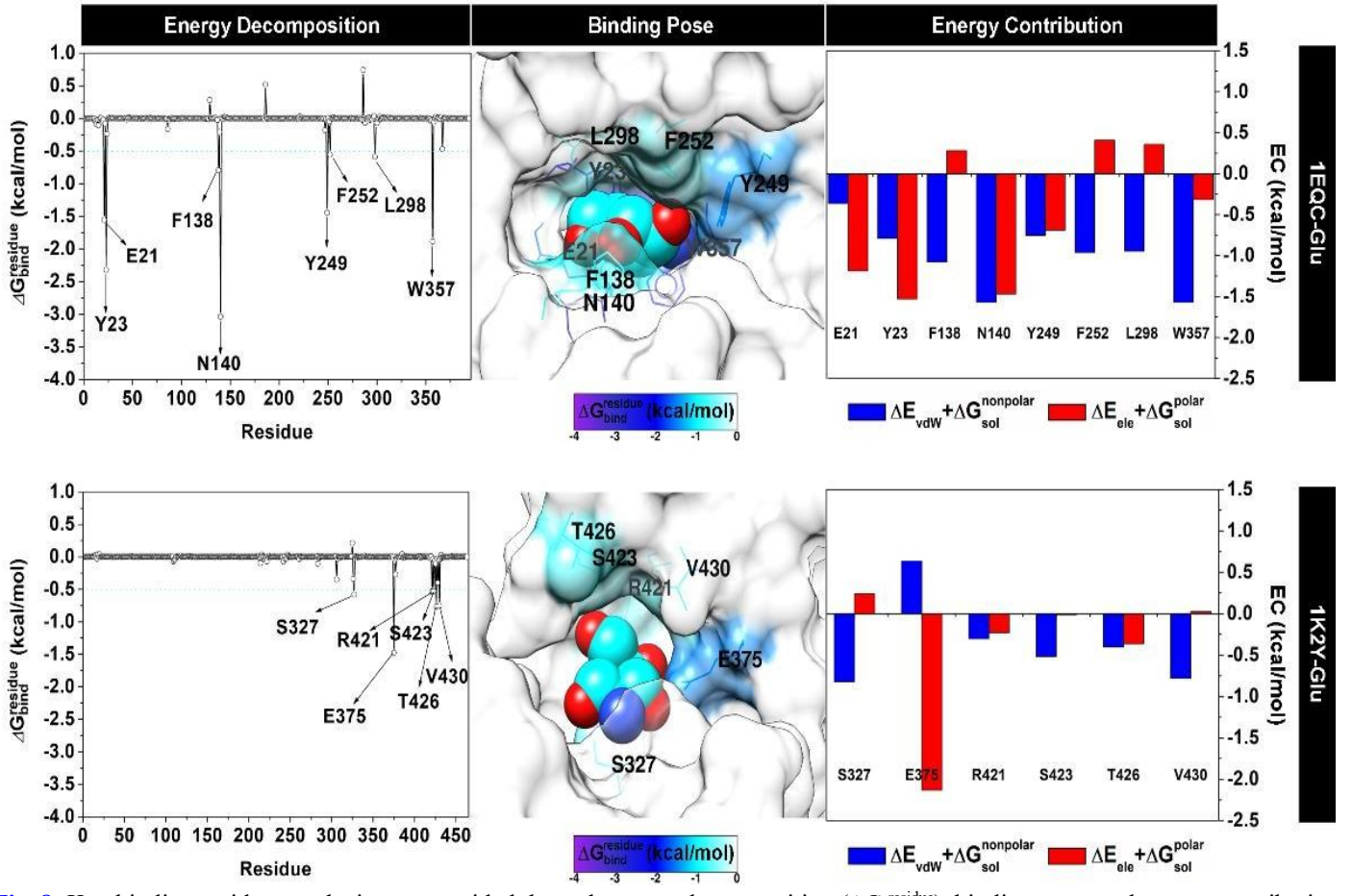

Fig. 8: Key binding residues analysis was provided through energy decomposition ($\Delta G^{residue}$), binding pose, and energy contribution.

comprehensive data in viewing the dynamic behavior of each system. This investigation provides insight into the inhibitory mechanism of Glu as a potential inhibitor of BgL2 and PMM/PGM.

3.6 MIC of fluconazole and meropenem against mono- and poly-microbial planktonic *C. albicans* and *P. aeruginosa*

MIC is the lowest concentration of an antibacterial agent, measured in mg/L or µg/mL, that completely prevents the growth of a test strain under strictly controlled *in vitro* conditions. In this study, we followed the protocol from EUCAST to first determine the MIC of meropenem and fluconazole as single compounds,[29] as well as in combination, against planktonic *C. albicans* and *P. aeruginosa*. Based on the experiment shown in Fig. S6, the MIC of meropenem against a planktonic culture of *P. aeruginosa* was 0.5, while the MIC of fluconazole against *C. albicans* was 0.125. The MICs of meropenem and fluconazole against mixed cultures of planktonic *C. albicans* and *P. aeruginosa* were 0.25 and 0.031, respectively (Fig. S7). These values were demonstrated by color changes at these concentrations, indicating the lowest concentration at which the drugs begin to affect *C. albicans* and *P. aeruginosa*. The MIC values from the co-culture were used as reference values to assess their effect as antibiofilm agents and in combination therapy to enhance the performance of fluconazole and meropenem against their *C. albicans-P. aeruginosa* biofilm.

3.7 Influence of glucosamine on the effectivity of fluconazole and meropenem

The effect of glucosamine on the antimicrobial performance of meropenem and fluconazole was assessed by measuring the amount of ECM in the *C. albicans* and *P. aeruginosa* PMBFs, determining the number of CFUs within the biofilm and conducting qualitative measurements using SEM. As shown in the histogram in (Fig. 9A), 10% glucosamine improved the effectiveness of meropenem against *C. albicans-P. aeruginosa* PMBFs. Including 10% glucosamine during treatment with meropenem at 4- and 8-fold the MIC suppressed *P. aeruginosa* in the biofilm. In contrast, when exposed to meropenem at 4- and 8-fold the MIC without glucosamine, the number of CFUs of *P. aeruginosa* was 500 cells/µL, while the inclusion of 10% glucosamine completely eliminated them (0 cells/µL). These data indicate that glucosamine actively enhances the effectiveness of meropenem (Fig. 9B).

As shown in (Fig. 9C), fluconazole at 4- and 8-fold the MIC allowed the number of *C. albicans* colonies to reach approximately 500 cells/µL, but the addition of 10% glucosamine completely eliminated *P. aeruginosa*. These results demonstrate the significant role of glucosamine in enhancing the antifungal activity of fluconazole against *C. albicans* under conditions where a biofilm was induced. In

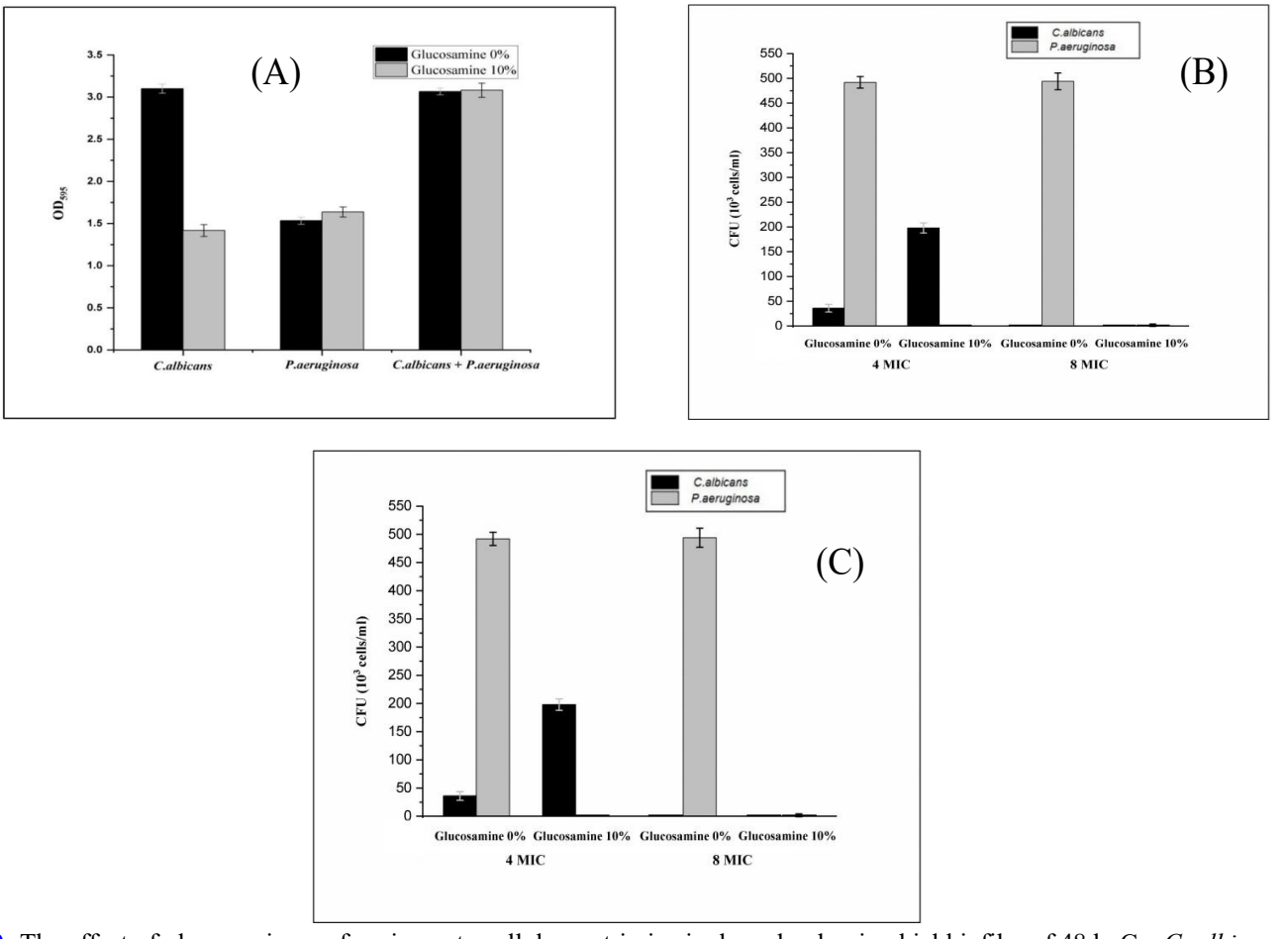

Fig. 9: The effect of glucosamine on forming extracellular matrix in single and polymicrobial biofilm of 48 h. Ca: *C. albicans*; Pa: *P. aeruginosa*; Ca+Pa: *C. albicans-P. aeruginosa* as measured using the crystal violet method at OD595. (A) The effects of glucosamine on the activity of meropenem at 48 h against the polymicrobial biofilm of *C. albicans-P. aeruginosa* grown in a 96-well microtiter plate, measured by the total plate count method. Meropenem used at 4 × MIC and 8 × MIC, while fluconazole was at 1 × MIC; (B) The effects of glucosamine on the activity of fluconazole at 48 h against the polymicrobial biofilm of *C. albicans-P. aeruginosa* grown in a 96-well microtiter plate, measured by the total plate count method; and (C) Fluconazole was used at 4 × MIC and 8 × MIC while using meropenem at 1 × MIC.

general, biofilms are formed when microbial cells need to protect themselves from adverse conditions, such as nutrient deprivation, the presence of antimicrobial agents (including antibiotics), and the host's immune system.

3.8 SEM confirmed the effects of glucosamine

The SEM profile of the *C. albicans-P. aeruginosa* biofilm, shown in (Fig. 10), suggests an interaction between the two species due to their proximity. This phenomenon may be attributed to syntrophy or cross-feeding, where one species feeds on the metabolic products of another through electron transfer to overcome energy limitations.[30,31] In this type of interaction, the transfer of metabolites can occur between two or more metabolically diverse species living in close proximity to each other.[32]

The effects of glucosamine were demonstrated by comparing the SEM images of the PMBFs with and without glucosamine (Fig. 11). In the absence of glucosamine, *P. aeruginosa* (smaller cells) and *C. albicans* (larger cells) formed large and extensive aggregates, resulting in the formation of a biofilm (Fig. 11A). In contrast, in the presence of 10% glucosamine, almost all *C.albicans* and *P. aeruginosa* cells were in their free form (Fig. 11B), referred to as freely planctonics.

A combination antimicrobial therapy against the *C. albicans-P. aeruginosa* PMBFs have been reported, demonstrating an inefficient performance despite the highest antimicrobial dose; even after 24 h of treatment, both microbial species existed in the form of a consortium.[5] In addition, administering high antimicrobial doses and exceeding clinical recommendations was highly toxic to humans. PolyB and AmB demonstrated synergistic effects against the mixed planktonic cultures of *P. aeruginosa* or *C. albicans*. However, only very high doses of PolyB, 256 mg/L (256 × MIC), affected PMBFs, with a loss of cultivability but not viability in *P. aeruginosa* at 2 h post-treatment, while the inhibition of *C. albicans* only started after 14 h. In this study, glucosamine with antibiofilm activity was used as a concomitant agent with fluconazole and meropenem against a *C. albicans* - *P. aeruginosa* PMBFs at low concentrations, 4

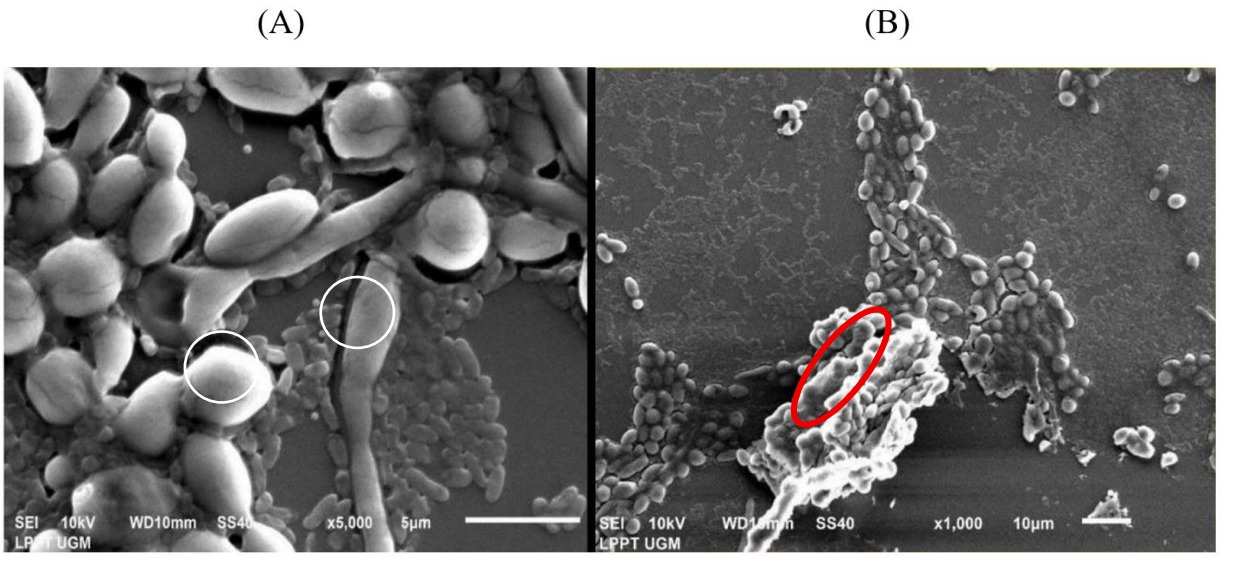

Fig. 10: SEM profile of the *C. albicans-P. aeruginosa* biofilm, at 5000× (A) and 1000× (B) magnification, attached to the surface of a 96-well microtiter plate. White circle: association between *C. albicans-P. aeruginosa*, red circle: biofilm with the thickest matrix.

× MIC of fluconazole and 1 × MIC meropenem.

Glucosamine is a precursor of peptidoglycan in bacteria and a component of glucosaminoglycans in eukaryotes. In addition, glucoseamine is a safe food supplement with little or no toxicity against human cell cultures used to support the structure and proper functioning of joints and treat and relieve osteoarthritis pain. Glucosamine is a nonprescription drug. Glucosamine demonstrated a remarkable antibiofilm activity against both mono- and polymicrobial biofilms of *Pseudomonas aeruginosa* and *Candida albicans*. Therefore, it can be a good candidate for use as an inclusion agent to treat lung infections, especially VAP. It also can be used to treat other polymicrobial biofilm such as cystic fibrosis, otitis media and urinary and tract infections.[33]

There have been many research reports with the aim of discovering new anti-biofilm agents from natural sources.[34] Natural products from plants, microorganisms, and marine organisms are unpredictable sources of anti-biofilm agents. Therefore, a top-down research strategy is needed to explore anti-biofilm agents from natural sources. There are many examples of top-down approachs, including the approach of screening, isolating and characterizing alkaloids from marine sponges that are active against gram-positive and gram-negative bacteria.[35] Another example is the isolation and characterization of styrylpyrone and quinic acid derivatives from Helichrysum italicum polar extract, which are active against *P. aeruginosa* and pholretin,[36] to reduce the formation of enterohemorrhagic *Escherichia coli* O157:H7 (EHEC) biofilms.[37] The top down research strategy, besides requiring a long time, often does not succeed in obtaining novel or new target compounds. Even though they have succeeded in isolating, characterizing and purifying natural anti-biofilm agents. Although they have succeeded in isolating, characterizing and purifying natural anti-biofilm agents, most

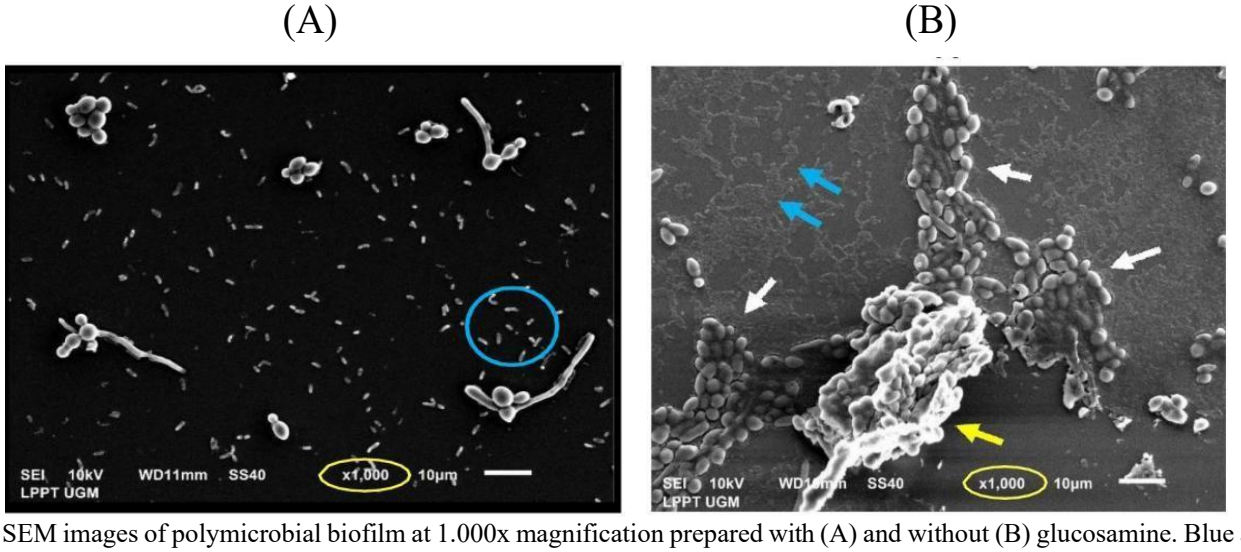

Fig. 11: SEM images of polymicrobial biofilm at 1.000x magnification prepared with (A) and without (B) glucosamine. Blue arrows: *P. aeruginosa* biofilm. White arrows: *C. albicans* biofilm. Yellow arrows: *C. albicans* biofilm with the thickest extracellular matrix. Blue circle: Free planktonic cells.

of the long step isolation processes produce very small yields. As has been done by researchers in an article exploring anti-biofilm agents from nature.[38–40]

Meanwhile, the bottom-up method has been successfully carried out in this research to explore extracellular matrix-based antibiofilm. We have discovered glucosamine as new antibiofilm towards both and mix C. albicans and P. aeruginosa by using this method. The collection of small molecules that will be tested in the *in silico* experiments were based on several criteria, including non-toxic, easy to produce in unlimited quantities and as far as possible from natural ingredients. We can choise materials that are suitable for production as non-hazardous medicinal ingredients at an early step. In the future, easily available glucosamine can be developed for application in many cases of infectious diseases involving *C. albicans*-*P. aeruginosa* polymicrobial that is difficult to treat until now as they are opportunistic pathogens capable of producing biofilms in clinical devices. These two pathogens are frequently found at the site of device-associated nosocomial infections, including ventilator-associated pneumonia (VAP), bloodstream and urinary tract infections.[41] Lung infections with *P. aeruginosa* often appear as secondary infections following primary lung infections with *C. albicans*.[42] In cystic fibrosis (CF) patients, cocolonizations of *C. albicans*-*P. aeruginosa* are often found. This kind of co-infection in CF and VAP cases is associated with prolonged hospital stay, decreased lung function, and high mortality in the intensive care unit (ICU).[43-49]

4. Conclusion

In conclusion, glucosamine has been developed as an extracellular matrix-targeting antibiofilm agent against *P. aeruginosa*-*C. albicans* biofilms using a simple bottom-up method. Exposure of *P. aeruginosa* and *C. albicans* mixed biofilms to a combination of the antibiotics meropenem and fluconazole at MICs of 4 and 8 times, respectively, without glucosamine caused the number of *P. aeruginosa* and *C. albicans* colonies to reach approximately 500 cells/µL (CFU). In contrast, the same exposure with the addition of 10% glucosamine completely eliminated the colonies. The inclusion of glucosamine as an antibiofilm agent in combination therapy with antibiotics and/or antifungals presents an attractive therapeutic option fo treating severe bacterial-fungal polymicrobial infections, such as pneumonia. These infections frequently involve colonization of endotracheal tube surfaces, where *C. albicans* and *P. aeruginosa* form drug-resistant polymicrobial biofilms (PMBFs).

Acknowledgements

This work was supported by Directorates Riset, Teknologi, dan Pengabdian kepada Masyarakat, who have provided research grant of Kolaborasi Penelitian Strategis (Katalis) 2024, SK Number: 0664/E5/PG.02.00/2024.

Conflict of Interest

There is no conflict of interest.

Supporting Information

Applicable.

References

[1] M. Hamet, A. Pavon, F. Dalle, A. Pechinot, S. Prin, J. P. Quenot, P. E. Charles, Candida spp. airway colonization could promote antibiotic-resistant bacteria selection in patients with suspected ventilator-associated pneumonia, *Intensive Care Medicine*, 2012, **38**, 1272-1279, doi: 10.1007/s00134-012-2584-2.

[2] M. A. Jabra-Rizk, Pathogenesis of polymicrobial biofilms, *The Open Mycology Journal*, 2011, **5**, 39-43, doi: 10.2174/1874437001105010039.

[3] H. Hamzah, T. Hertiani, S. U. T. Pratiwi, T. Nuryastuti, The inhibition activity of tannin on the formation of mono-species and polymicrobial biofilm *Escherichia coli*, *Staphylococcus aureus*, *Pseudomonas aeruginosa*, and *Candida albicans*, *Majalah Obat Tradisional*, 2019, **24**, 110, doi: 10.22146/mot.44532.

[4] H. N. Bandara, D. A. Wood, I. Vanwonterghem, P. Hugenholtz, B. K. Cheung, L. P. Samaranayake, Fluconazole resistance in *Candida albicans* is induced by *Pseudomonas aeruginosa* quorum sensing, *Scientific Reports*, 2020, **10**, 7769, doi: 10.1038/s41598-020-64761-3.

[5] M. E. Rodrigues, S. P. Lopes, C. R. Pereira, N. F. Azevedo, A. Lourenço, M. Henriques, M. O. Pereira, Polymicrobial ventilator-associated pneumonia: fighting in vitro *Candida albicans*–*Pseudomonas aeruginosa* biofilms with antifungal–antibacterial combination therapy, *PLoS One*, 2017, **12**, e0170433, doi: 10.1371/journal.pone.0170433.

[6] A. Baktir, H. Suwito, M. Safinah, B. Kunsah, Novel materials for eradication of biofilm extracellular matrix of pathogenic Candida, *Journal of Materials Science and Engineering: B*, 2012, **2**, 650-658.

[7] D. Santosaningsih, Y. M. S. Poejiani, R. F. Putri, L. Dewi, H. Arifani, Y. L. Ni'mah, A. Baktir, The biofilm inhibition properties of glucosamine gold nanoparticles in combination with meropenem against Pseudomonas aeruginosa on the endotracheal tube: a model of biofilm-related ventilator-associated pneumonia, *Materials*, 2024, **17**, 1604, doi: 10.3390/ma17041604.

[8] S. M. Cutfield, G. J. Davies, G. Murshudov, B. F. Anderson, P. C. E. Moody, P. A. Sullivan, J. F. Cutfield, The structure of the exo-β-(1,3)-glucanase from *Candida albicans* in native and bound forms: relationship between a pocket and groove in family 5 glycosyl hydrolases, *Journal of Molecular Biology*, 1999, **294**, 771-783, doi: 10.1006/jmbi.1999.3287.

[9] C. Regni, P. A. Tipton, L. J. Beamer, Crystal structure of PMM/PGM: an enzyme in the biosynthetic pathway of *P. aeruginosa* virulence factors, *Structure*, 2002, **10**, 269-279, doi: 10.1016/S0969-2126(02)00705-0.

[10] D. E. V. Pires, T. L. Blundell, D. B. Ascher, pkCSM: predicting small-molecule pharmacokinetic and toxicity properties using graph-based signatures, *Journal of Medicinal*

Chemistry, 2015, **58**, 4066-4072, doi: 10.1021/acs.jmedchem.5b00104.
[11] A. Daina, O. Michielin, V. Zoete, SwissADME: a free web tool to evaluate pharmacokinetics, drug-likeness and medicinal chemistry friendliness of small molecules, *Scientific Reports*, 2017, **7**, 42717, doi: 10.1038/srep42717.
[12] S. R. Brozell, S. Mukherjee, T. E. Balius, D. R. Roe, D. A. Case, R. C. Rizzo, Evaluation of DOCK 6 as a pose generation and database enrichment tool, *Journal of Computer-Aided Molecular Design*, 2012, **26**, 749-773, doi: 10.1007/s10822-012-9565-y.
[13] W. J. Allen, T. E. Balius, S. Mukherjee, S. R. Brozell, D. T. Moustakas, P. T. Lang, D. A. Case, I. D. Kuntz, R. C. Rizzo, DOCK 6: Impact of new features and current docking performance, *Journal of Computational Chemistry*, 2015, **36**, 1132-1156, doi: 10.1002/jcc.23905.
[14] V. Salmaso, S. Moro, Bridging molecular docking to molecular dynamics in exploring ligand-protein recognition process: an overview, *Frontiers in Pharmacology*, 2018, **9**, 923, doi: 10.3389/fphar.2018.00923.
[15] D. A. Case, H. M. Aktulga, K. Belfon, D. S. Cerutti, G. A. Cisneros, V. W. D. Cruzeiro, AmberTools: a suite of programs for molecular dynamics simulations, *Journal of Chemical Information and Modeling*, 2023, **63**, 6183-6191, doi: 10.1021/acs.jcim.3c01153.
[16] Z. Zhang, W. Lu, AmberMDrun: A scripting tool for running amber MD in an easy way, *Biomolecules*, 2023, **13**, 635, doi: 10.3390/biom13040635.
[17] B. R. Miller III, T. D. McGee Jr, J. M. Swails, N. Homeyer, H. Gohlke, A. E. Roitberg, MMPBSA.py: an efficient program for end-state free energy calculations, *Journal of Chemical Theory and Computation*, 2012, **8**, 3314-3321, doi: 10.1021/ct300418h.
[18] E. Wang, H. Sun, J. Wang, Z. Wang, H. Liu, J. Z. H. Zhang, T. Hou, End-point binding free energy calculation with MM/PBSA and MM/GBSA: strategies and applications in drug design, *Chemical Reviews*, 2019, **119**, 9478-9508, doi: 10.1021/acs.chemrev.9b00055.
[19] G. Batoni, G. Maisetta, S. Esin, Microbial biofilms and antibiofilm agents 2.0, *International Journal of Molecular Sciences*, 2022, **23**, 7932, doi: 10.3390/ijms23147932.
[20] H. Y. Hussein, A. H. Hasan, A. J. Hussein, M. M. Ayoob, M. K. Samad, N. H. Hussen, F. E. Hawaiz, S. Shakya, S. Muzaffar, J. Jamalis, Novel pyrazoline-thiazole hybrids containing azo group as antibacterial agents: design, synthesis, in vitro bioactivity, in silico molecular docking, ADME profile and DFT studies, *Research on Chemical Intermediates*, 2024, **50**, 4551-4578, doi: 10.1007/s11164-024-05354-x.
[21] H. M. Al-Maqtari, A. H. Hasan, M. Suleiman, M. A. Ahmad Zahidi, M. A. Noamaan, P. Alexyuk, M. Alexyuk, A. Bogoyavlenskiy, J. Jamalis, Benzyloxychalcone hybrids as prospective acetylcholinesterase inhibitors against Alzheimer's disease: rational design, synthesis, in silico ADMET prediction, QSAR, molecular docking, DFT, and molecular dynamic simulation studies, *ACS Omega*, 2024, **9**, 32901-32919, doi: 10.1021/acsomega.4c03679.
[22] M. A. A. Orabi, A. H. Hasan, S. F. AbouZid, D. El Amir, M. H. Hetta, A. A. Al Awadh, O. S. Alqahtani, T. Hatano, M. A. El-Shanawany, Nutritional, antioxidant, antimicrobial, and anticholinesterase properties of Phyllanthus emblica: a study supported by spectroscopic and computational investigations, *Metabolites*, 2023, **13**, 1013, doi: 10.3390/metabo13091013.
[23] D. Chen, N. Oezguen, P. Urvil, C. Ferguson, S. M. Dann, T. C. Savidge, Regulation of protein-ligand binding affinity by hydrogen bond pairing, *Science Advances*, 2016, **2**, e1501240, doi: 10.1126/sciadv.1501240.
[24] T. Lippert, M. Rarey, Fast automated placement of polar hydrogen atoms in protein-ligand complexes, *Journal of Cheminformatics*, 2009, **1**, 13, doi: 10.1186/1758-2946-1-13.
[25] X. Meng, H. Zhang, M. Mezei, M. Cui, Molecular docking: a powerful approach for structure-based drug discovery, *Current Computer Aided-Drug Design*, 2011, **7**, 146-157, doi: 10.2174/157340911795677602.
[26] D. R. Roe, T. E. Cheatham III, PTRAJ and CPPTRAJ: software for processing and analysis of molecular dynamics trajectory data, *Journal of Chemical Theory and Computation*, 2013, **9**, 3084-3095, doi: 10.1021/ct400341p.
[27] Y. Maruyama, R. Igarashi, Y. Ushiku, A. Mitsutake, Analysis of protein folding simulation with moving root mean square deviation, *Journal of Chemical Information and Modeling*, 2023, **63**, 1529-1541, doi: 10.1021/acs.jcim.2c01444.
[28] M. Y. Lobanov, N. S. Bogatyreva, O. V. Galzitskaya, Radius of gyration as an indicator of protein structure compactness, *Molecular Biology*, 2008, **42**, 623–628, doi: 10.1134/S0026893308040195.
[29] X. Du, Y. Li, Y. Xia, S.-M. Ai, J. Liang, P. Sang, X. Ji, S. Liu, Insights into protein-ligand interactions: mechanisms, models, and methods, *International Journal of Molecular Sciences*, 2016, **17**, 144, doi: 10.3390/ijms17020144.
[30] S. A. Hollingsworth, R. O. Dror, Molecular dynamics simulation for all, *Neuron*, 2018, **99**, 1129-1143, doi: 10.1016/j.neuron.2018.08.011.
[31] J. Schiebel, R. Gaspari, T. Wulsdorf, K. Ngo, C. Sohn, T. E. Schrader, A. Cavalli, A. Ostermann, A. Heine, G. Klebe, Intriguing role of water in protein-ligand binding studied by neutron crystallography on trypsin complexes, *Nature Communications*, 2018, **9**, 3559, doi: 10.1038/s41467-018-05769-2.
[32] I. Lukac, P. G. Wyatt, I. H. Gilbert, F. Zuccotto, Ligand binding: evaluating the contribution of the water molecules network using the Fragment Molecular Orbital method, *Journal of Computer-Aided Molecular Design*, 2021, **35**, 1025-1036, doi: 10.1007/s10822-021-00416-3.
[33] B. G. Levine, J. E. Stone, A. Kohlmeyer, Fast analysis of molecular dynamics trajectories with graphics processing units: Radial distribution function histogramming, *Journal of Computational Physics*, 2011, **230**, 3556–3569, doi: 10.1016/j.jcp.2011.01.048.
[34] T. Schön, J. Werngren, D. Machado, E. Borroni, M. Wijkander, G. Lina, J. Mouton, E. Matuschek, G. Kahlmeter, C.

Giske, M. Santin, D. M. Cirillo, M. Viveiros, E. Cambau, Antimicrobial susceptibility testing of Mycobacterium tuberculosis complex isolates-the EUCAST broth microdilution reference method for MIC determination, *Clinical Microbiology and Infection*, 2020, **26**, 1488-1492, doi: 10.1016/j.cmi.2020.07.036.
[35] Y. Kamagata, Syntrophy in anaerobic digestion, Anaerobic Biotechnology: Environmental Protection and Resource Recovery, London: Imperial College Press, 2015, 13-30, ISBN: 978-1-78326-789-7.
[36] L. Hao, T. Y. Michaelsen, C. M. Singleton, G. Dottorini, R. H. Kirkegaard, M. Albertsen, P. H. Nielsen, M. S. Dueholm, Novel syntrophic bacteria in full-scale anaerobic digesters revealed by genome-centric metatranscriptomics, *The ISME Journal*, 2020, **14**, 906-918, doi: 10.1038/s41396-019-0571-0.
[37] E. Rosenberg, E. F. DeLong, S. Lory, E. Stackebrandt, F. Thompson, The Prokaryotes: Prokaryotic Communities and Ecophysiology, Berlin, Heidelberg: Springer-Verlag, 2013, 528, ISBN: 978-3-642-30122-3.
[38] C. B. Ibberson, M. Whiteley, The social life of microbes in chronic infection, *Current Opinion in Microbiology*, 2020, **53**, 44-50, doi: 10.1016/j.mib.2020.02.003.
[39] J. Masák, A. Čejková, O. Schreiberová, T. Řezanka, Pseudomonas biofilms: possibilities of their control, *FEMS Microbiology Ecology*, 2014, **89**, 1-14, doi: 10.1111/1574-6941.12344.
[40] S. D. Stowe, J. J. Richards, A. T. Tucker, R. Thompson, C. Melander, J. Cavanagh, Anti-biofilm compounds derived from marine sponges, *Marine Drugs*, 2011, **9**, 2010-2035, doi: 10.3390/md9102010.
[41] B. D'Abrosca, E. Buommino, G. D'Angelo, L. Coretti, M. Scognamiglio, V. Severino, S. Pacifico, G. Donnarumma, A. Fiorentino, Spectroscopic identification and anti-biofilm properties of polar metabolites from the medicinal plant *Helichrysum italicum* against *Pseudomonas aeruginosa*, *Bioorganic & Medicinal Chemistry*, 2013, **21**, 7038-7046, doi: 10.1016/j.bmc.2013.09.019.
[42] J. H. Lee, S. C. Regmi, J.-A. Kim, M. H. Cho, H. Yun, C. S. Lee, J. Lee, Apple flavonoid phloretin inhibits *Escherichia coli* O157:H7 biofilm formation and ameliorates colon inflammation in rats, *Infection and Immunity*, 2011, **79**, 4819-4827, doi: 10.1128/IAI.05580-11.
[43] S. M. Brackett, K. E. Cox, S. L. Barlock, W. M. Huggins, D. F. Ackart, R. J. Bassaraba, R. J. Melander, C. Melander, Meridianin D analogues possess antibiofilm activity against *Mycobacterium smegmatis*, *RSC Medicinal Chemistry*, 2020, **11**, 92-97, doi: 10.1039/c9md00466a.
[44] B. M. Fontaine, K. Nelson, J. T. Lyles, P. B. Jariwala, J. M. García-Rodriguez, C. L. Quave, E. E. Weinert, Identification of ellagic acid rhamnoside as a bioactive component of a complex botanical extract with anti-biofilm activity, *Frontiers in Microbiology*, 2017, **8**, 496, doi: 10.3389/fmicb.2017.00496.
[45] M. S. Hifnawy, H. M. Hassan, R. Mohammed, M. M. Fouda, A. M. Sayed, A. A. Hamed, S. F. AbouZid, M. E. Rateb, H. A. Alhadrami, U. R. Abdelmohsen, Induction of antibacterial metabolites by co-cultivation of two Red Sea sponge-associated actinomycetes *Micromonospora* sp. UR56 and *Actinokinespora* sp. EG49, *Marine Drugs*, 2020, **18**, 243, doi: 10.3390/md18050243.
[46] G. Menon, A. Subramanian, P. Baby, N. Daniel, R. Radhika, M. George, S. Menon, Incidence of device-associated healthcare-associated infections from a neurosurgical intensive care unit of a tertiary care center: A retrospective analysis, *Anesthesia, Essays and Researches*, 2020, **14**, 454-460, doi: 10.4103/aer.AER_112_20.
[47] D. Huang, M. Qi, Y. Hu, M. Yu, Z. Liang, The impact of *Candida* spp airway colonization on clinical outcomes in patients with ventilator-associated pneumonia: A systematic review and meta-analysis, *American Journal of Infection Control*, 2020, **48**, 695-701, doi: 10.1016/j.ajic.2019.11.002.
[48] M. Al Shakirchi, L. Klingspor, P. Bergman, L. Hjelte, I. de Monestrol, A 16-year retrospective study on fungal prevalence and diversity in patients with cystic fibrosis: *Candida dubliniensis* was associated with a decline in lung function, *International Journal of Infectious Diseases*, 2020, **96**, 663-670, doi: 10.1016/j.ijid.2020.05.063.
[49] Y. Huang, Y. Jiao, J. Zhang, J. Xu, Q. Cheng, Y. Li, S. Liang, H. Li, J. Gong, Y. Zhu, L. Song, Z. Rong, B. Liu, Z. Jie, S. Sun, P. Li, G. Wang, J. Qu, Infection Assembly of Shanghai Respiratory Society, Microbial etiology and prognostic factors of ventilator-associated pneumonia: A multicenter retrospective study in Shanghai, *Clinical Infectious Diseases*, 2018, **67**, S146-S152, doi: 10.1093/cid/ciy686.